

Measurement of $\Upsilon(1S)$ Production at *BABAR*

Inclusive Measurement at the $\Upsilon(4S)$

by

Rocky Yat Cheung So

A THESIS SUBMITTED IN PARTIAL FULFILMENT OF
THE REQUIREMENTS FOR THE DEGREE OF

Bachelor of Science

in

The Faculty of Science

(Honours Biophysics)

The University Of British Columbia

(Vancouver, Canada)

April 14th, 2008

© Rocky Yat Cheung So 2008

Abstract

BABAR is a particle physics experiment at the Stanford Linear Accelerator Center (SLAC). The purpose of *BABAR* is to study matter-antimatter asymmetry in the bottom quark system. At SLAC, electrons and positrons collide, which annihilate and decay into a variety of daughters. An $\Upsilon(4S)$ meson is one of the possible daughters. An $\Upsilon(4S)$ decays into a B meson and \bar{B} meson more than 96% of the time. A B meson has an anti-bottom quark and a \bar{B} meson has a bottom quark. The purpose of this thesis is to measure how many $\Upsilon(1S)$ originated from $\Upsilon(4S)$ in the entire *BABAR* data set. This thesis compares on-peak data and off-peak data. On-peak data was taken at center of mass energy 10.58GeV . One of the possible interactions is $e^+e^- \rightarrow \Upsilon(4S)$ since the mass of $\Upsilon(4S)$ is $10.58\text{GeV}/c^2$. Off-peak data, taken at center of mass energy 10.54GeV , is not enough to have any $B\bar{B}$ pairs because 10.54GeV is less than the mass of an $\Upsilon(4S)$. This thesis can be useful for *BABAR* physicist because it helps set an upper limit on how many $B\bar{B}$ pairs there are in the entire *BABAR* data set. In other words, it sets an upper limit on how much more than 96% does $\Upsilon(4S)$ decay to $B\bar{B}$. Measurement the decay of $\Upsilon(4S) \rightarrow \Upsilon(1S) + X$ give evidence for non $B\bar{B}$ decays of the $\Upsilon(4S)$. The final results of this study shows that there were $(110 \pm 3) \times 10^5$ $\Upsilon(1S)$ on-peak, of which $(10 \pm 9) \times 10^5$ originated from an $\Upsilon(4S)$. Increasing the centre of mass energy from 10.54GeV to 10.58GeV increases the $\Upsilon(1S)$ production by $(10 \pm 8)\%$.

Table of Contents

Abstract	ii
Table of Contents	iii
List of Tables	v
List of Figures	vi
Acknowledgements	vii
1 Introduction	1
1.1 Overview of the <i>BABAR</i> Experiment	1
1.2 Anatomy of SLAC	1
1.3 The <i>BABAR</i> Coordinate System	2
1.4 Laboratory Frame and Centre of Mass Frame	3
1.5 Bottomonium	3
1.6 Motivation for the Measurement of $\Upsilon(1S)$ at $\Upsilon(4S)$	4
2 Particle Interactions	6
3 Data	9
3.1 Physics of Muon and Electron Identification	9
3.2 Candidates Selection	10
3.3 Monte Carlo Sample	11
4 Analysis Procedures	12
4.1 Detector Resolution	12
4.2 $\Upsilon(1S)$	13
4.3 Detection Efficiencies	14
4.4 Angular Distributions of Monte Carlo Samples	16
4.5 Angular Distribution of Detected $\Upsilon(1S)$	16
4.6 Calculated Number of Events Expected	21
4.6.1 ISR Events	21
4.6.2 Feed Down Events	21
5 Results	24
5.1 Comparison of On-peak and Off-peak Data	24
5.2 Error Analysis	25

Table of Contents

5.3 Attempt to Measure χ_{bJ} (3P)	25
5.4 Attempt to Measure $\Upsilon(2S)$ and $\Upsilon(3S)$	26
Bibliography	30
 Appendices	
A Comparison of SP1072 and SP3981	31

List of Tables

2.1	Mass of Υ species.	7
3.1	Summary of the data sets, versions used, integrated luminosities, and number of $\Upsilon(4S)$ in each Run.	9
3.2	Angles selection in laboratory frame and centre of mass frame.	11
3.3	Summary of Monte Carlo sample used.	11
4.1	Detection efficiencies of different signal Monte Carlo types of different Runs.	16
4.2	Υ dielectron widths and ISR cross sections.	22
4.3	Number of ISR Υ produced and decayed into muon pairs.	22
4.4	Number of $\Upsilon(1S)$ from known feed down events.	23
5.1	Summary of uncertainties.	25
5.2	χ_{bJ} (3P) masses and energy of the photon that decayed with it.	25

List of Figures

1.1	SLAC and the PEP-II Rings	1
1.2	The <i>BABAR</i> detector	2
1.3	The <i>BABAR</i> coordinates system.	2
1.4	<i>BABAR</i> boost protractor.	4
1.5	A spectrum of bottomonium species.	4
2.1	Feynman diagram of the quark pair and lepton pair production	6
2.2	Flow chart of on-peak processes.	8
2.3	Flow chart of off-peak processes.	8
3.1	Ratio of E/p for particles of different energies.	10
4.1	Invariant mass of muon pairs.	12
4.2	Data VS background Monte Carlo at $M_{\Upsilon(1S)}$	13
4.3	Number of $\Upsilon(1S) \rightarrow \mu^+\mu^-$ detected on-peak.	14
4.4	Number of $\Upsilon(1S) \rightarrow \mu^+\mu^-$ detected off-peak.	15
4.5	Background Monte Carlo angular distributions in the forward direction.	17
4.6	Background Monte Carlo angular distributions in the backward direction	17
4.7	Angular distribution at signal region and outside signal region.	18
4.8	Angular distribution of detected $\Upsilon(1S)$ on-peak	19
4.9	Angular distribution of detected $\Upsilon(1S)$ off-peak	20
5.1	Invariant mass of two muons plus one photon greater than 500MeV	27
5.2	On-peak data and background Monte Carlo at $\Upsilon(2S)$ region.	27
5.3	On-peak data and background Monte Carlo at $\Upsilon(3S)$ region.	28
5.4	On-peak data minus background Monte Carlo at $\Upsilon(2S)$ region.	28
5.5	Off-peak data minus background Monte Carlo at $\Upsilon(2S)$ region.	29
A.1	On-peak comparison of muon angular distribution.	31
A.2	Off-peak comparison of muon angular distribution.	31
A.3	On-peak differences of muon angular distribution between data and Monte Carlo.	32
A.4	Off-peak differences of muon angular distribution between data and Monte Carlo.	32

Acknowledgements

I would like to thank Dr. Christopher Hearty for the many hours he spent supervising this research. He identified the project and gave me brilliant ideas for this data analysis.

Also, thanks to Doug Maas for setting up and maintaining the computer I used for the analysis, and thanks to Dr. Robert Kiefl and Dr. Michael Hasinoff for coordinating the Physics 449 course.

Finally, I would like to thank my family for their support, especially my father, Wing Keung So, who always reminds me to do my best and never give up.

Chapter 1

Introduction

1.1 Overview of the *BABAR* Experiment

The *BABAR* experiment takes place at the Stanford Linear Accelerator Center (SLAC) in California, USA. It studies matter-antimatter asymmetry in the bottom quark system. Mesons are produced in SLAC by colliding positrons to electrons head on at speeds close to the speed of light. Electrons are accelerated to 9GeV and positrons are accelerated to 3.1GeV . Since electrons and positrons are each other's anti-particle, they annihilate when they hit each other, making an $\Upsilon(4S)$ particle a fraction of the time. This $\Upsilon(4S)$ particle subsequently decays into a pair of B mesons (one B and one \bar{B}). These are what *BABAR* physicists are interested in. By studying the differences between how a B and a \bar{B} evolve, *BABAR* physicists can better understand the matter-antimatter asymmetry, which can help explain why the universe is dominated with matter instead of antimatter.

1.2 Anatomy of SLAC

SLAC has an accelerator and a detector. The accelerator is linear and injects electrons and positrons into the Positron Electron Project II (PEP-II) ring. The detector is made of many different components. Figure 1.1 [1] shows how the linac feeds electrons and positrons into two separate rings.

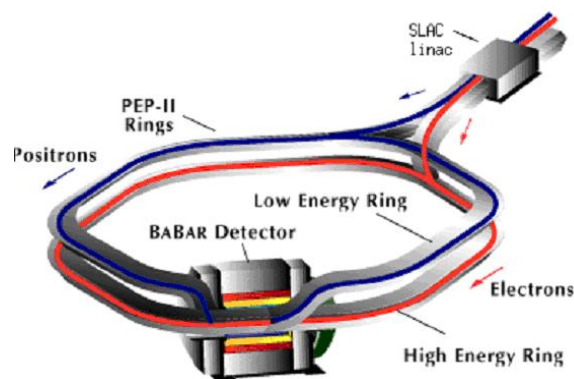
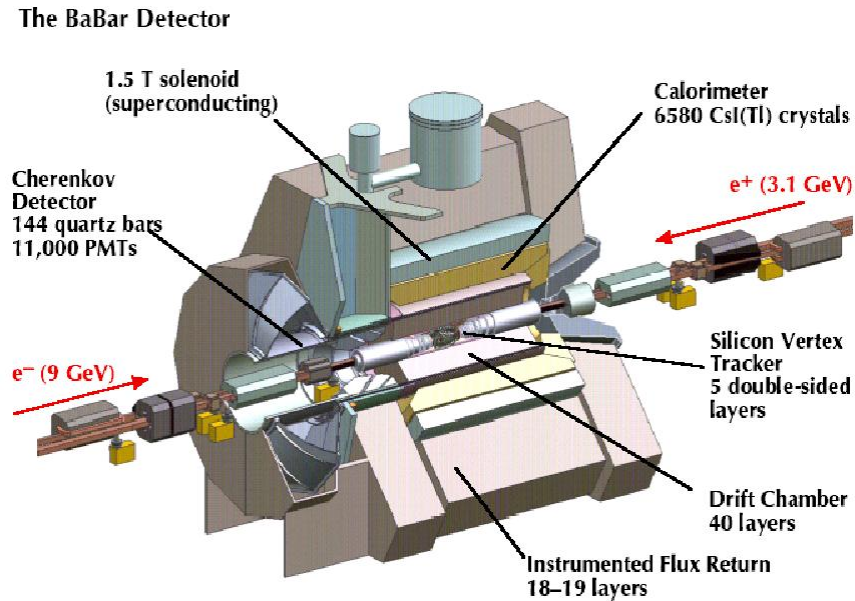
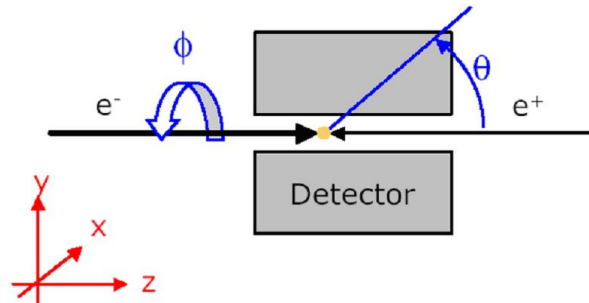


Figure 1.1: SLAC and the PEP-II Rings

Using electromagnetic fields, electrons and positrons are accelerated down the linac and moved into the PEP-II rings where they begin to travel in opposite directions. The two beams are steered to hit each other at the *BABAR* detector, where data is taken.

Figure 1.2: The *BABAR* detectorFigure 1.3: The *BABAR* coordinates system.

The *BABAR* detector is able to identify and measure the energy, momentum, azimuthal angle ϕ , and polar angle θ of a charged track. It has five different detectors to do this as shown in Figure 1.2 [1]. The Silicon Vertex Tracker records where the track originates (where the vertex of an interaction is). The Drift Chamber measures the momentum of a track. The Detector of Internally Reflected Cherenkov light detects and identifies hadrons. The Cesium Iodide calorimeter measures photon energies. Finally, the Instrumented Flux Return identifies muons and neutral hadrons.

1.3 The *BABAR* Coordinate System

Throughout this thesis, the *BABAR* coordinates convention will be used (see Figure 1.3). The z-axis points in the direction of the electron beam. The x-axis horizontally points away from the PEP-II ring. θ is the angle a charged track makes with the z-axis. ϕ is the angle a charged track makes with the x-axis in the x-y plane.

1.4 Laboratory Frame and Centre of Mass Frame

In the laboratory frame, the electrons are accelerated to 9GeV and positrons to 3.1GeV. After their collision, the $\Upsilon(4S)$ continues to move in the electron's initial direction for momentum to be conserved. The *BABAR* experiment is designed to do this so we can resolve the decay vertex of the B mesons. Since the total mass of $B\bar{B}$ is 10.54GeV[4], $B\bar{B}$ move almost as fast as the $\Upsilon(4S)$ in the laboratory frame. If the electron and positron beams are symmetric in the laboratory frame, then the B mesons would decay at the centre of mass and we cannot see which one decayed first.

We can Lorentz transform from the laboratory frame to the centre of mass frame. At the GeV scale, electrons and positrons can be considered massless (m is zero in Einstein's energy momentum relation $E^2 = p^2c^2 + m^2c^4$).

Lab Frame

$$9GeV e^- \rightarrow \leftarrow 3.1GeV e^+$$

$$\text{Energy of collision} = 12.1GeV = E$$

$$\text{Momentum of collision} = 5.9GeV = p_z$$

Centre of Mass Frame

$$5.29GeV e^- \rightarrow \leftarrow 5.29GeV e^+$$

$$\text{Energy of collision} = 10.58GeV = E'$$

$$\text{Momentum of collision} = 0GeV = p'_z$$

$$\begin{aligned} p'_z &= \gamma(p_z - \beta E) \\ \beta &= p_z/E = 0.487 \\ \gamma &= 1.15 \\ \beta\gamma &= 0.56 \end{aligned}$$

Therefore, the centre of mass frame is travelling along the z-axis at about half the speed of light relative to the laboratory frame. This thesis analyses muon data in the centre of mass frame. The relationship between θ in the laboratory frame and θ' in the centre of mass frame is:

$$\cos\theta' = (\cos\theta - \beta)/(1 - \beta\cos\theta) \quad (1.1)$$

Azimuthal angle does not change in a boost along the z axis.

$$\phi' = \phi \quad (1.2)$$

Figure 1.4 shows how θ in one frame is related to the other.

1.5 Bottomonium

Bottomonium is a general term that applies to any meson that has one bottom quark and one anti-bottom quark. States with different quantum numbers have different names. For example, a bottomonium with quantum numbers $J^{PC} = 1^{--}$ is called an Υ , where J is the total angular momentum, P is the parity quantum number, and C is the charge conjugation quantum number. A χ_{bJ} is a bottomonium with quantum number $J^{PC} = 0, 1, 2^{++}$. J can be 0, 1, or 2, which

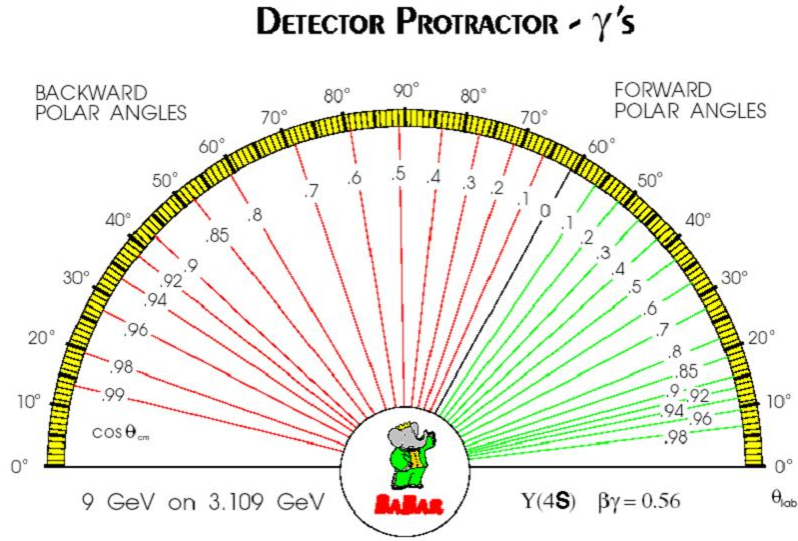


Figure 1.4: BABAR boost protractor.

corresponds to three states for each of the $\chi_{bJ}(mP)$. Figure 1.5 [2] shows different bottomonium species, their respective quantum numbers, and a few of their decay modes.

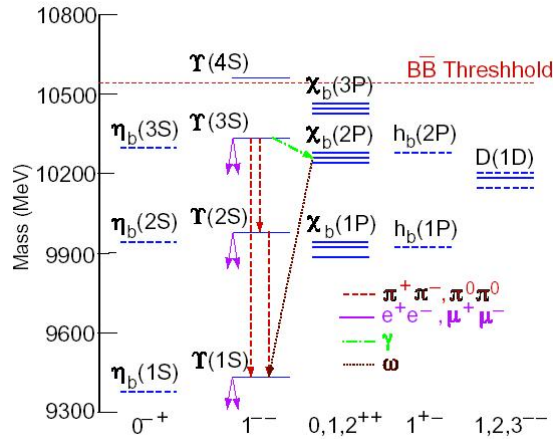


Figure 1.5: A spectrum of bottomonium species.

1.6 Motivation for the Measurement of $\Upsilon(1S)$ at $\Upsilon(4S)$

BABAR physicists are interested in B mesons. At BABAR, $B\bar{B}$ pairs are created by the production of an $\Upsilon(4S)$. $\Upsilon(4S)$ decays into $B\bar{B}$ mesons more than 96% of the time (95% confidence interval) [3]. BABAR physicists would like to know how many B mesons there are in the entire BABAR data set. Therefore, if we can measure how often an $\Upsilon(4S)$ decays into an $\Upsilon(1S)$, it gives us more information on the upper limit of how many $B\bar{B}$ mesons were produced. The BABAR experiment

took data at two energies: on-peak ($\sqrt{s} = 10.58\text{GeV}$) and off-peak ($\sqrt{s} = 10.54\text{GeV}$). An $\Upsilon(4S)$ has a mass of 10.58GeV , so on-peak data can have $\Upsilon(4S)$ in them. Off-peak energy is slightly below that required to make an $\Upsilon(4S)$, so $\Upsilon(4S)$ would not be present in the data. By comparing the two data sets, the number of $\Upsilon(1S)$ decayed from an $\Upsilon(4S)$ can be measured.

The branching fraction $\mathcal{B}(\Upsilon(4S) \rightarrow \Upsilon(1S) + \text{anything})$ is measured to be less than 4×10^{-3} [3]. The measurement of this thesis is not a branching fraction. It is an inclusive measurement that includes any $\Upsilon(1S)$ that originated from an $\Upsilon(4S)$ regardless of whether it decayed into a χ_{bJ} , $\Upsilon(3S)$, or $\Upsilon(2S)$ first, or directly to $\Upsilon(1S)$ in the process.

This thesis also attempts to show evidence for χ_{bJ} in the 3P state. This state has never been observed directly before.

Heavy quarkonia interactions are important for testing of lattice quantum chromodynamics (LQCD). Many heavy quarkonia are studied by measuring their decays. The $\Upsilon(4S)$ is above open flavour threshold. Thus, this study can be useful for LQCD theorists.

Chapter 2

Particle Interactions

At *BABAR*, an electron-positron collision annihilates and makes a virtual photon, which decays into quark pairs or lepton pairs. Figure 2.1 are the Feynman diagrams for the two interactions.

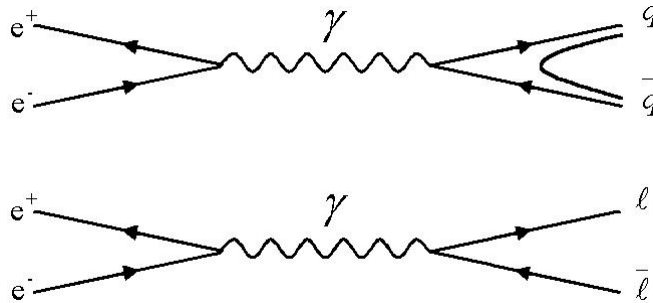


Figure 2.1: Feynman diagram of the quark pair and lepton pair production. The first Feynman diagram is the production of quark-antiquark pairs. The second Feynman diagram is the production of lepton-antilepton pairs. Time goes from left to right.

When a quark pair is produced, they hadronize [4]. In the case of bottom quark pairs, they hadronize to an Υ . Since the quantum numbers of a photon and an Υ are both $J^{PC} = 1^{--}$, Υ is the only bottomonium species that can be made. Thus, a χ_{bJ} cannot be made initially.

At such high energies, photons can be emitted from any of the four legs in the above Feynman diagrams. The photon would carry away some energy and momentum. If the photon was emitted in the two initial legs, the collision would have energy less than the 10.58GeV or 10.54GeV .

$$\begin{aligned} e^+e^- &\rightarrow \gamma q\bar{q} \\ e^+e^- &\rightarrow \gamma \ell^+\ell^- \end{aligned}$$

Any photon emitted from a lepton prefers to point along the direction of its parent lepton. Therefore, if a photon is emitted initially, the lepton final states would also preferentially point in the initial directions. $e^+e^- \rightarrow \gamma \mu^+\mu^-$ has an angular distribution peaked in the forward and backward directions.

If a bottom quark pair is created, an $\Upsilon(4S)$ can be made only if there were no photons. It would be completely stationary in the centre of mass frame. If a photon is emitted before the collision, it would carry away some energy and there would not be enough energy to make an $\Upsilon(4S)$. However, $\Upsilon(nS)$, where $n = 1, 2, 3$, can be made even if a photon carried away some energy. This is because the masses of $\Upsilon(nS)$ are lower than the energy of the collision. The masses of Υ species are given in Table 2.1 [3].

In this process, the photon associated with an $\Upsilon(nS)$, is called an initial state radiation photon, or γ_{ISR} .

	Mass (GeV)
$\Upsilon(1S)$	9.46030 ± 0.00026
$\Upsilon(2S)$	10.02326 ± 0.00031
$\Upsilon(3S)$	10.3552 ± 0.0005
$\Upsilon(4S)$	10.5794 ± 0.0012

Table 2.1: Mass of Υ species.

$$e^+e^- \rightarrow \gamma\Upsilon(nS)$$

In the off-peak data set, many of the Υ particles come from the ISR process. The others come from the feed down of intermediate decays such as $\Upsilon(3S) \rightarrow X \rightarrow \Upsilon(1S)$.

Similarly, in the on-peak data set, there are many $\Upsilon(nS)$ from the ISR process, but there are also decays from the $\Upsilon(4S)$. One of these known decays is $\Upsilon(4S) \rightarrow \pi^+\pi^-\Upsilon(nS)$ [5].

There are even more feed down processes because an $\Upsilon(4S)$ may decay into $\Upsilon(3S)$ or other bottomonium species, which may end up decaying into an $\Upsilon(1S)$. Figure 1.5 shows how an $\Upsilon(3S)$ can decay into $\gamma + \chi_{b2}(2P)$, which may subsequently decays into $\omega + \Upsilon(1S)$. Figure 1.5 is a simplification of the cascade of events that can make a $\Upsilon(1S)$. In reality, there are many more intermediate decays possible.

This thesis analyses muon data collected in the *BABAR* experiment. There are many *background* muon events in the form of $e^+e^- \rightarrow \gamma\mu^+\mu^-$. We are interested in the *signal* events. These events come from Υ decays into muon pairs $\Upsilon(1S) \rightarrow \mu^+\mu^-$.

The *BABAR* experiment recorded muon energies and momenta for every event. This gives their 4-momentum vector. Adding the muons' 4-momenta and squaring it gives the invariant mass squared. If the two muons decayed from an $\Upsilon(1S)$, this would necessarily be equal to the mass of an $\Upsilon(1S)$.

$$(p_{\mu^+} + p_{\mu^-})^2 = M_{\Upsilon(1S)}^2$$

Figures 2.2 and 2.3 summarizes the processes relevant to this thesis.

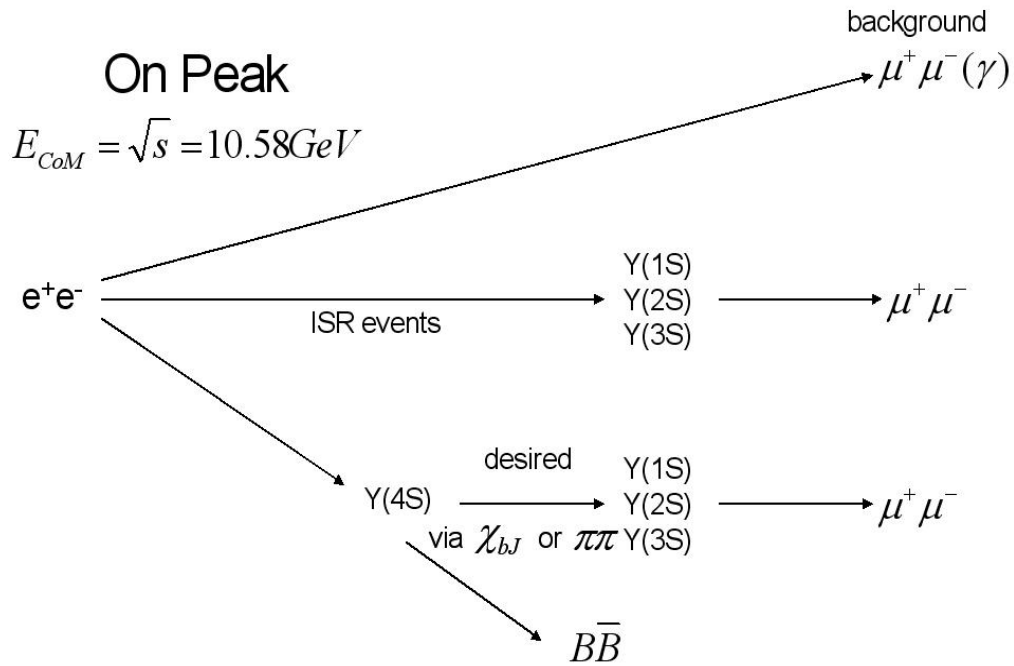


Figure 2.2: Flow chart of on-peak processes.

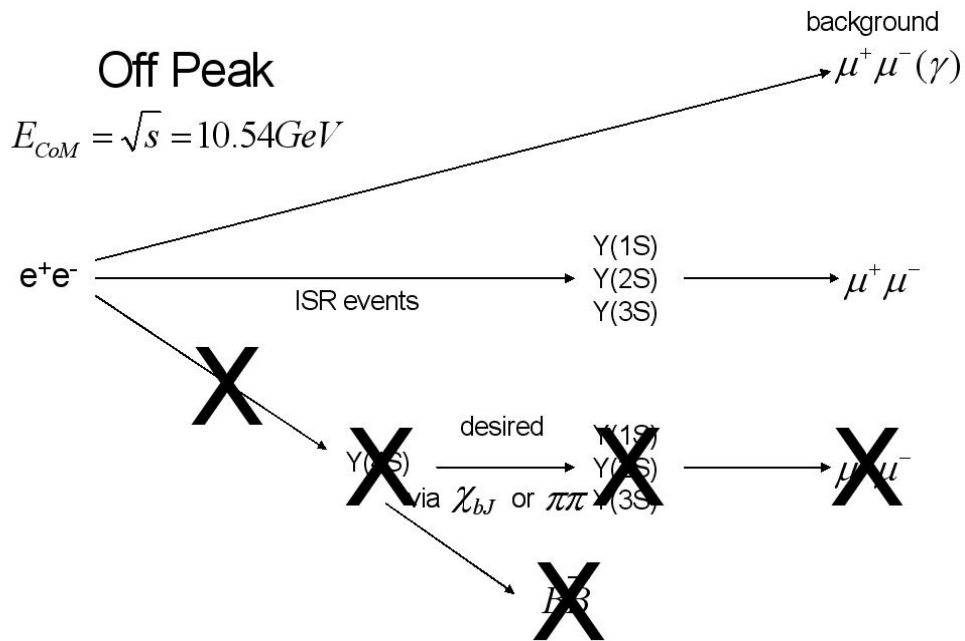


Figure 2.3: Flow chart of off-peak processes.

Chapter 3

Data

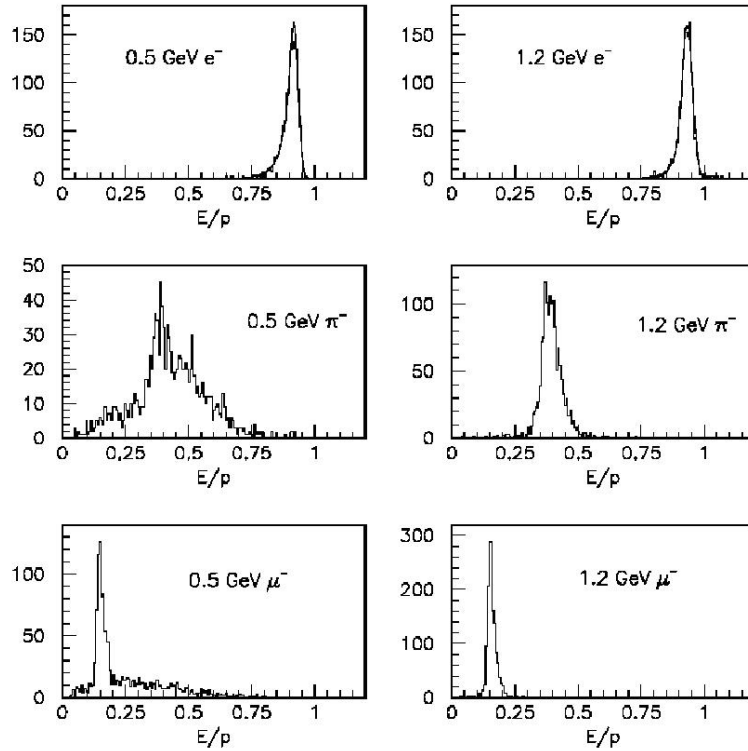
The *BABAR* experiment started taking data in 1999. It takes data for 9 months in a year. Each year's data set is called a Run. This analysis uses data from Run 1 to Run 6. Table 3.1 summarizes the data sets used in this analysis.

Data Set	Integrated Luminosity (pb^{-1})	Number of $\Upsilon(4S)$ (10^6)
AllEventsSkim-Run1-OffPeak-R22d-v07	2620	0
AllEventsSkim-Run2-OffPeak-R22d-v07	6920	0
AllEventsSkim-Run3-OffPeak-R22d-v04	2470	0
AllEventsSkim-Run4-OffPeak-R22d-v07	10100	0
AllEventsSkim-Run5-OffPeak-R22d-v07	14500	0
AllEventsSkim-Run6-OffPeak-R22d-v07	7280	0
Total Off-Peak Data	43900	0
AllEventsSkim-Run1-OnPeak-R22d-v07	20400	22.39 ± 0.25
AllEventsSkim-Run2-OnPeak-R22d-v07	61100	67.39 ± 0.74
AllEventsSkim-Run3-OnPeak-R22d-v04	32300	35.57 ± 0.39
AllEventsSkim-Run4-OnPeak-R22d-v07	100000	110.45 ± 1.22
AllEventsSkim-Run5-OnPeak-R22d-v07	133000	147.19 ± 1.62
AllEventsSkim-Run6-OnPeak-R22d-v07	76200	82.04 ± 0.90
Total On-Peak Data	423000	465.04 ± 5.15

Table 3.1: Summary of the data sets, versions used, integrated luminosities, and number of $\Upsilon(4S)$ in each Run.

3.1 Physics of Muon and Electron Identification

The *BABAR* detector measures leptons as charged tracks. When a high energy electron moves through a medium, it can emit a photon. This photon can subsequently create an electron-positron pair by pair production. The electron and positron can further emit photons, which will produce pairs and so on until the particles have insufficient energy to produce more particles. This phenomenon is called electromagnetic shower [6]. Muons and electrons have distinct shower shapes. By analyzing the shape of a shower, a detector can identify an electron from a muon. The ratio of the energy deposited in a shower to the momentum of the electron, E/pc , is nearly one[7]. This means that electrons deposit most of their energy in its shower. However, since muons do not shower like electrons, they deposit a lot less energy as electrons. The E/pc ratio and distribution are characteristic for different particles. Figure 3.1 [7] shows how different particles deposit different amounts of energy.

Figure 3.1: Ratio of E/p for particles of different energies.

3.2 Candidates Selection

The major goal of this analysis is to measure how many $\Upsilon(1S)$ there are in the on-peak data set.

Data in the *BABAR* experiment are recorded as individual events. Data used in this analysis are muon events that satisfy the following:

- there were two charged tracks originating from one vertex,
- one of the charged tracks was identified as a muon,
- the two charged tracks had total energies that range from 8 to 12 GeV in the centre of mass frame,
- and the event passed the BGFmumu filter (a reconstructing software filter that roughly identifies dimuon events $e^+e^- \rightarrow \mu^+\mu^-$).

The *BABAR* detector is cylindrical. It “wraps” around the beam pipe and there are no detectors along the beam direction. *BABAR* is known to be capable of measuring polar angles θ from 0.41 to 2.54 radians in the laboratory frame. The corresponding angles in the centre of mass frame are given in Table 3.2.

Along with the above criteria, muons with $\cos\theta$ from -0.78 to 0.78 were selected instead of from -0.94 to 0.78. This is done to avoid any bias from having more muons in the backwards direction of the data set.

θ (radians)	$\cos\theta$	θ' (radians)	$\cos\theta'$
0.41	0.92	0.68	0.78
2.54	-0.83	2.78	-0.94

Table 3.2: Angles selection in laboratory frame and centre of mass frame.

The muon pairs are reconstructed to Υ candidates. The four-momentum of these candidates are simply the sum of the four-vector of the muon pair.

3.3 Monte Carlo Sample

Both the on-peak and off-peak data involve many different processes; some of which we know and some we do not know about. To model the *BABAR* data, Monte Carlo simulations were used. Monte Carlo simulations are useful because they can model different processes separately.

Monte Carlo sample comes from computer-generated events. These events are then modelled to go through the *BABAR* detector. It includes any resolution effects in the detector. It models if a detector will detect the charged tracks and if it will satisfy the reconstruction criteria. Table 3.3 summarizes the Monte Carlo samples used in this analysis. There are two different models for the background process SP1072 and SP3981. This study uses SP3981 because it is believed to be the better one. A comparison of SP1072 and SP3981 is given in Appendix A.

Decay Mode	SP modenum	Number of Events On-Peak	Number of Events Off-Peak
$\mu^+\mu^-(\gamma)$	1072	1.2096060×10^7	6.37691×10^5
$\mu^+\mu^-(\gamma)$	3981	2.837796×10^8	6.689054×10^7
$\Upsilon(4S) \rightarrow \pi^+\pi^-\Upsilon(nS) \rightarrow \pi^+\pi^-\ell^+\ell^-$	5467	145000	0
$\Upsilon(4S) \rightarrow \gamma\chi_{bJ}(3P) \rightarrow \gamma\gamma\Upsilon(nS) \rightarrow \gamma\gamma\ell^+\ell^-$	8249	350000	0
$\gamma\Upsilon(nS) \rightarrow \gamma\ell^+\ell^-$	8268	1053000	0

Table 3.3: Summary of Monte Carlo sample used.

Chapter 4

Analysis Procedures

ROOT was used to analyse data from the *BABAR* database in ntuples format [8]. Figure 4.1 is a mass plot of the invariant muon pair mass on-peak and off-peak.

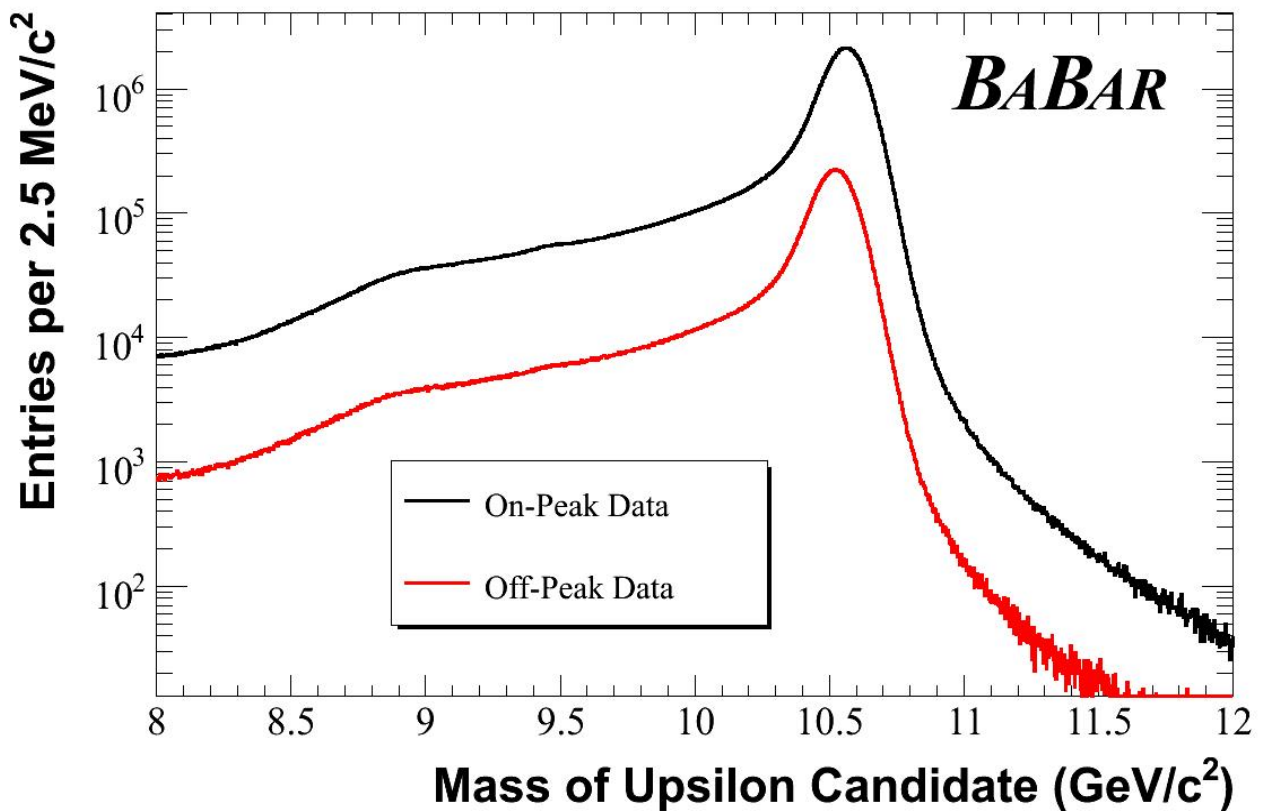


Figure 4.1: Invariant mass of muon pairs.

4.1 Detector Resolution

Most of the data are background events in the form of $e^+e^- \rightarrow \gamma\mu^+\mu^-$. The peaks of the two histograms occur slightly below their centre of mass energy because many events have lost energy via photon emission. It becomes an asymmetric Gaussian because events can only lose energy and move to the left side of the Gaussian instead of moving to the heavier side of the Gaussian.

The *BABAR* detector has a resolution. If an event had an invariant muon pair mass M , it is

going to be measured with a variance of σ^2 . The higher side of the Gaussian has energy higher than the centre of mass energy, so almost all the events there had no photons. The width of the higher energy side would be the approximate resolution of the detector because it is mostly events of centre of mass energy.

This width is approximately 70MeV . The detector's resolution is assumed to be constant from 8GeV to 12GeV .

4.2 $\Upsilon(1S)$

If the *BABAR* detector detects signal from $\Upsilon(1S)$, we expect to see an excess of events at the mass of $\Upsilon(1S)$ over background events. A Gaussian with mean at $M_{\Upsilon(1S)}$ and width σ is expected. The integral of this Gaussian would be the total number of $\Upsilon(1S)$ we detected.

The Monte Carlo for background events $e^+e^- \rightarrow \mu^+\mu^-\gamma$ is plotted with the data at the $\Upsilon(1S)$ region $\pm 4\sigma$. The mass region outside of 3σ have negligible signal. The Monte Carlo was scaled so the number of events at those regions is equal to the data. Those events are purely background events. Figure 4.2 shows the excess of events at the $\Upsilon(1S)$ region compared to background Monte Carlo.

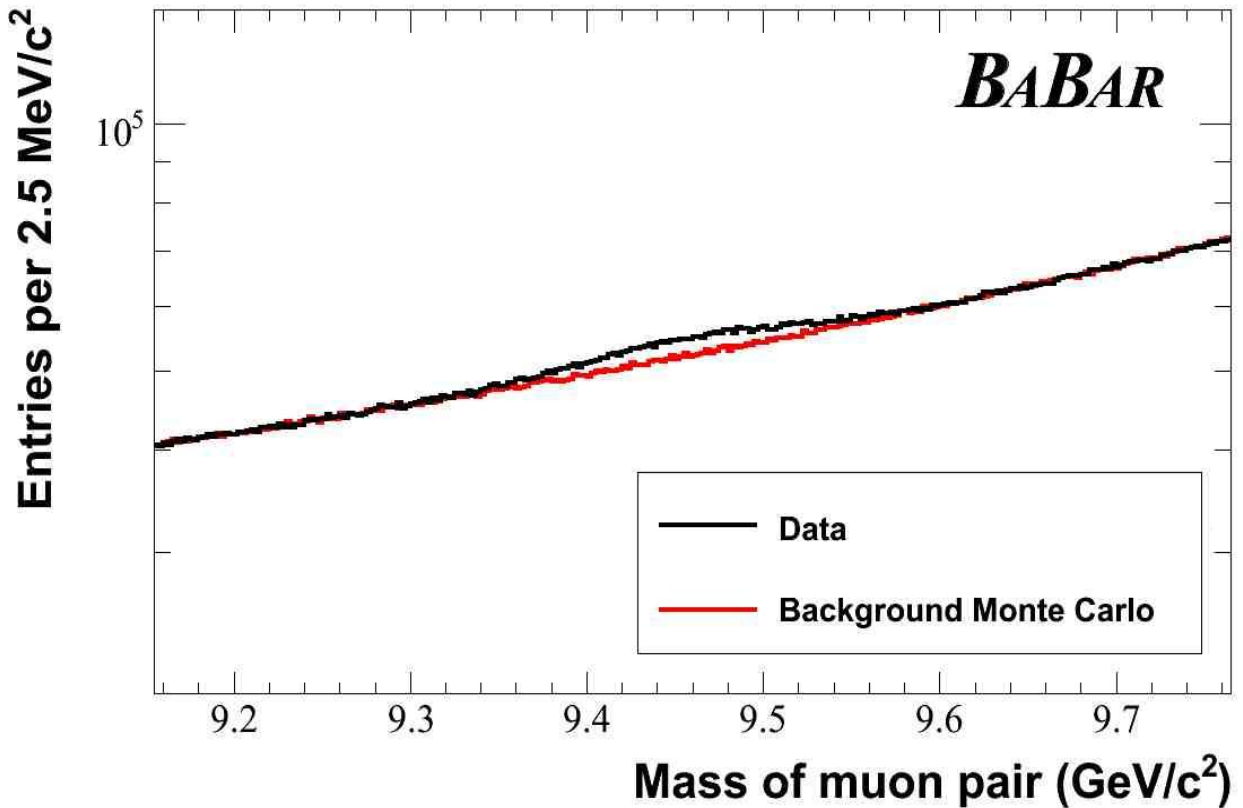


Figure 4.2: Data VS background Monte Carlo at $M_{\Upsilon(1S)}$

Then the background Monte Carlo events are subtracted from data to obtain the distribution

of signal events.

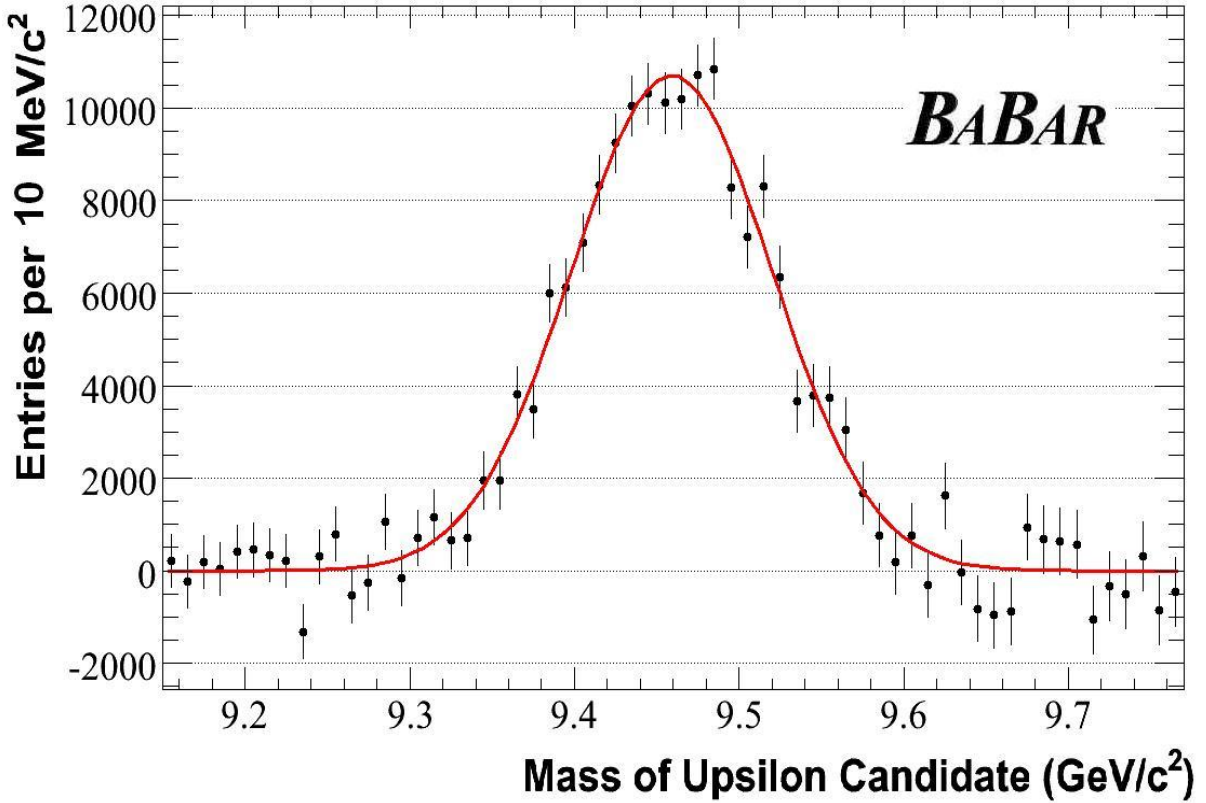


Figure 4.3: Number of $\Upsilon(1S) \rightarrow \mu^+\mu^-$ detected on-peak.

This was fitted to a Gaussian in Figure 4.3. There are $(1.644 \pm 0.04) \times 10^5$ $\Upsilon(1S) \rightarrow \mu^+\mu^-$ events in this Gaussian. Dividing this by the branching fraction $\mathcal{B}(\Upsilon(1S) \rightarrow \mu^+\mu^-) = (2.48 \pm 0.05)\%$, this corresponds to $(6.63 \pm 0.16) \times 10^6$ $\Upsilon(1S)$ detected.

The corresponding plot is given in Figure 4.4 for off-peak. There are $(6.5 \pm 0.4) \times 10^5$ $\Upsilon(1S)$ detected off-peak.

4.3 Detection Efficiencies

The number of $\Upsilon(1S)$ detected is less than the actual number of $\Upsilon(1S)$ produced because the *BABAR* detector has a detection efficiency less than 100%. Efficiencies are estimated using signal Monte Carlo sample.

Events were generated in signal Monte Carlo samples. As shown in Table 3.3, these were $\Upsilon(nS) \rightarrow \mu^+\mu^-$ events. Of these samples, Events that had an $\Upsilon(1S)$ generated and a muon pair generated right after were selected. These are the actual number of events of interest generated. Of these events, the exact same selection criteria used for candidate selection in data were applied. These events are the simulated events that survive to the detector and gets detected. Therefore, the efficiency ϵ is

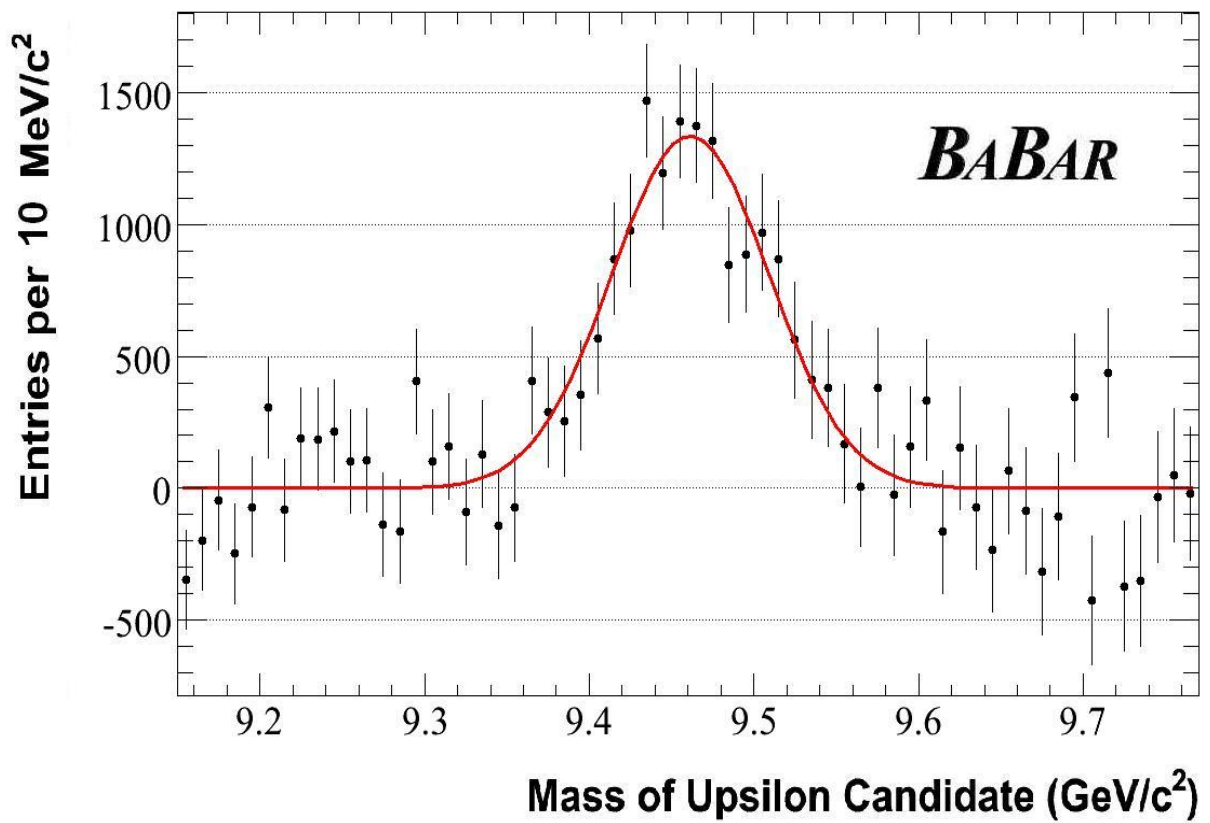


Figure 4.4: Number of $\Upsilon(1S) \rightarrow \mu^+\mu^-$ detected off-peak.

$$\epsilon = \frac{\#surviving}{\#generated} \quad (4.1)$$

These efficiencies are listed in Table 4.1 for different Runs for each signal Monte Carlo type. Their uncertainties are $\sqrt{n \times \epsilon(1 - \epsilon)}$, where n is the number of generated events of interest.

Run	$\Upsilon(4S) \rightarrow \pi\pi\Upsilon(nS)$	$\Upsilon(4S) \rightarrow \gamma\chi_{bJ}(3P) \rightarrow \gamma\gamma\Upsilon(nS)$	$\gamma_{ISR}\Upsilon(nS)$
1	0.668 ± 0.014	0.664 ± 0.012	0.592 ± 0.008
2	0.678 ± 0.008	0.670 ± 0.007	0.604 ± 0.005
3	0.679 ± 0.010	0.661 ± 0.010	0.601 ± 0.006
4	-	0.673 ± 0.005	0.605 ± 0.004
5	0.687 ± 0.005	0.668 ± 0.005	0.604 ± 0.003
6	0.679 ± 0.010	-	-

Table 4.1: Detection efficiencies of different signal Monte Carlo types of different Runs. Monte Carlo samples were not available for every Run.

Different signal types have different efficiencies because they have different angular distributions. The *BABAR* detector does not have a uniform detection efficiency over all polar angles.

4.4 Angular Distributions of Monte Carlo Samples

Knowing the number of $\Upsilon(1S)$ detected is not enough to determine if it decayed from an $\Upsilon(4S)$, decayed from a cascade of feed down events, or directly from an ISR event. Monte Carlo samples can be used to model the angular distributions of background events and different signal types.

The angular distribution of $\Upsilon(4S) \rightarrow \pi^+\pi^-\Upsilon(nS)$ and $\Upsilon(4S) \rightarrow \gamma\chi_{bJ}(3P) \rightarrow \gamma\gamma\Upsilon(nS)$ events are uniform. This is because in the event an $\Upsilon(4S)$ is made, it is stationary in the centre of mass frame. Its daughters would not inherit any momentum, and there is no preferred direction.

In ISR events, since an ISR photon carried away some momentum, the $\Upsilon(nS)$ particle is not stationary in the centre of mass frame when it gets created. ISR photons have angular distributions peaked in the forward and backward directions. To conserve momentum, the ISR photon and the Υ candidate would have to point back to back in the centre of mass frame.

Background Monte Carlo also have sharp spikes in the forwards and backwards region.

4.5 Angular Distribution of Detected $\Upsilon(1S)$

The shape angular distribution of detected $\Upsilon(1S)$ can tell what they are composed of. It is a combination of a uniform distribution of $\Upsilon(1S)$ decayed from $\Upsilon(4S)$ and a peaked distribution of ISR Υ . Since the number of background events is big compared to signal events, the accuracy of Monte Carlo angular distributions is very critical. In order to avoid any inaccurate modelling of the angular distribution of background events by Monte Carlo, data itself can also model the angular distributions of background events. The following is a description of how this was done.

Outside the signal region, since there is no $\Upsilon(1S)$, we can expect those events are purely background. That is, the events from $9.12 - 9.22\text{GeV}$ and $9.70 - 9.80\text{GeV}$ are expected to be

only $e^+e^- \rightarrow \gamma\mu^+\mu^-$. We expect that some combination of the lower region and the upper region of the data gives the angular distribution of the $e^+e^- \rightarrow \gamma\mu^+\mu^-$ at the signal region.

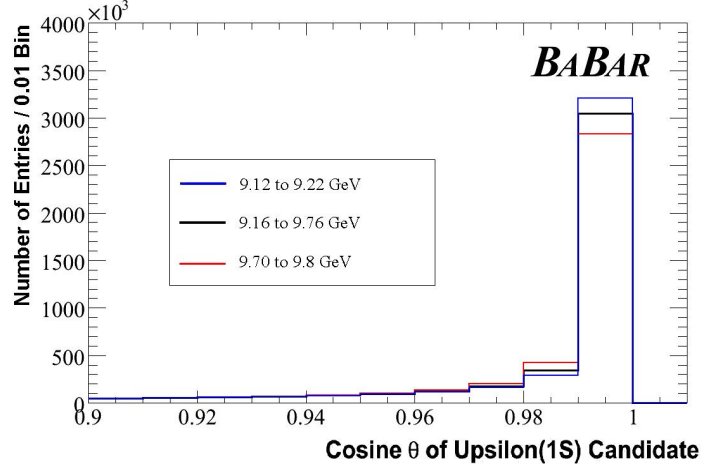


Figure 4.5: Background Monte Carlo angular distributions in the forward direction.

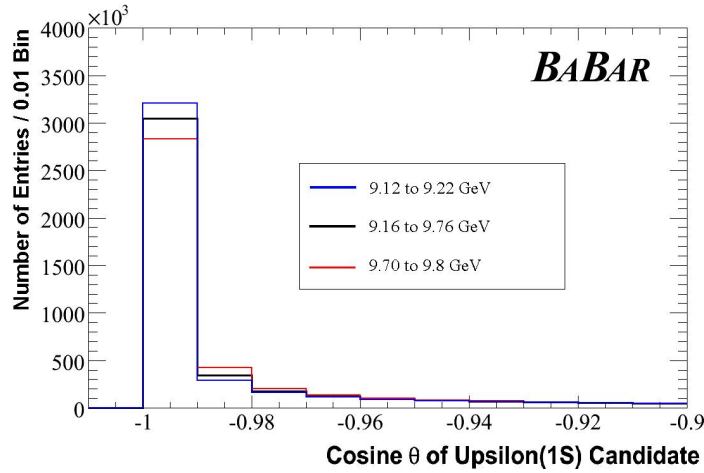


Figure 4.6: Background Monte Carlo angular distributions in the backward direction

To determine the weighting ratio, we looked at the angular distributions of background Monte Carlo and tried to emulate the signal region by adding the lower region to upper region with different proportions. The angular distributions in the forward and backwards region of background Monte Carlo are plotted in Figures 4.5 and 4.6. These plots show that lower the invariant mass, the more sharply peaked the angular distributions are in the forward and backward direction. By adding a $9.12 - 9.22\text{ GeV}$ distribution to a $9.70 - 9.80\text{ GeV}$ distribution, a new distribution that is almost identical to the one at signal region is obtained. The weighting was 53% lower region and 47% upper region. This weighting ratio was obtained by trial and error.

Using the outside regions does not give the exact angular distribution at the signal region. With background Monte Carlo, taking the actual angular distribution at the signal region and

subtracting the lower and upper region gives the disagreement. This disagreement should be similar to the disagreement for data.

In the actual *BABAR* data, 53% of the lower region and 47% of the upper region was added to the disagreement obtained from background Monte Carlo. Figure 4.7 is an on-peak plot of the angular distribution at signal region with the distribution outside the signal region. This is used as the angular distribution of $e^+e^- \rightarrow \gamma\mu^+\mu^-$ in the signal region.

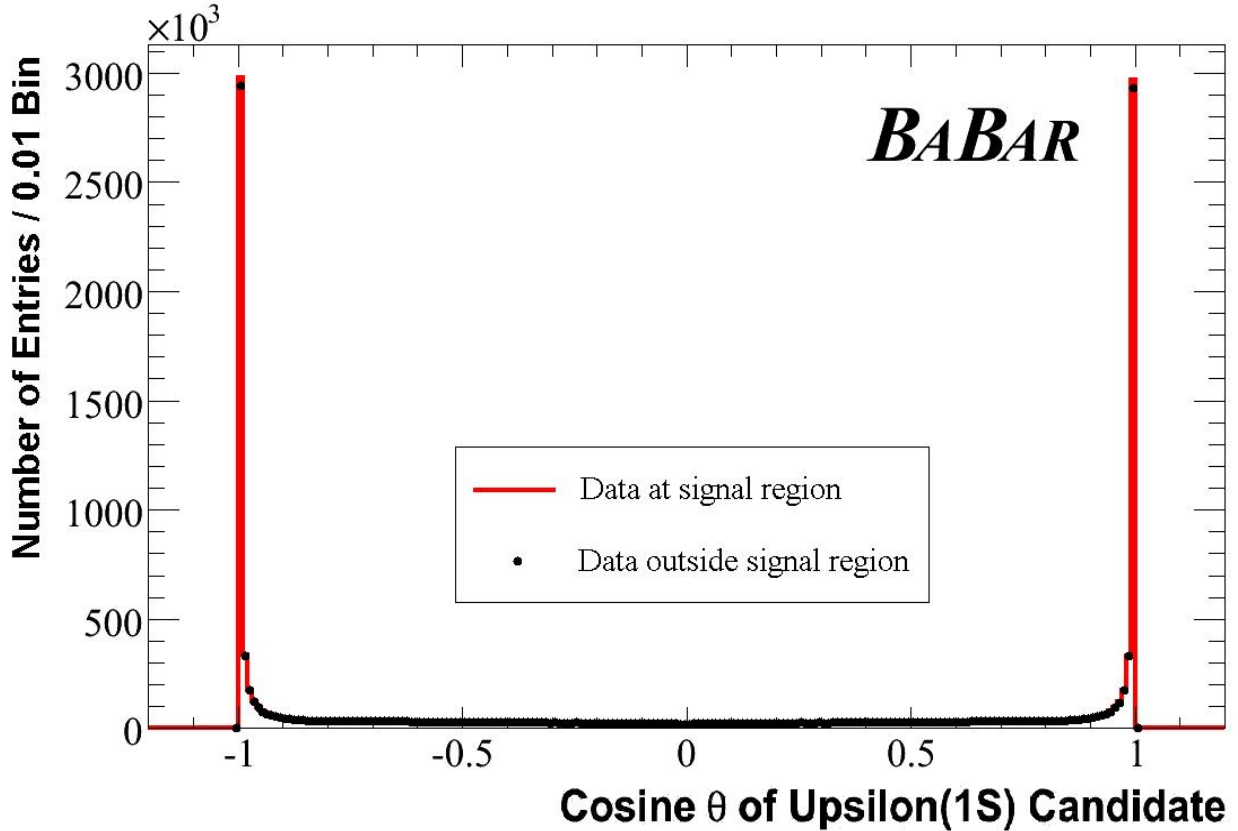


Figure 4.7: Angular distribution at signal region and outside signal region.

This was subtracted from the angular distribution of the data at the signal region. The resulting plot is the angular distribution of the detected $\Upsilon(1S)$. Figure 4.8 is on-peak and Figure 4.9 is off-peak.

The $\Upsilon(1S)$ in both the on-peak and off-data set is also peaked in the forward and backward region. This indicates that many of these are ISR Υ .

4.6 Calculated Number of Events Expected

4.6.1 ISR Events

ISR processes have been studied before [9] [10]. In these studies, the predicted cross section for ISR events were accurate up to the fine structure constant squared, α^2 .

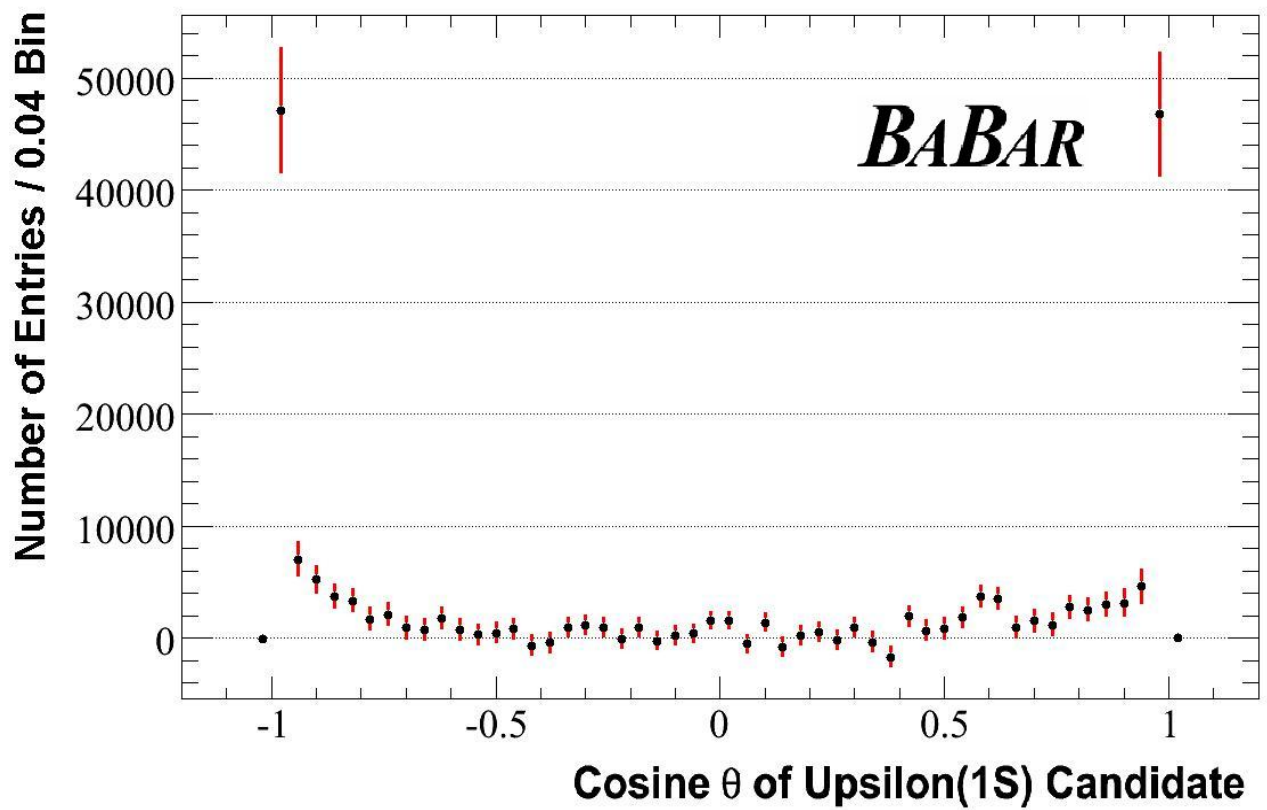


Figure 4.8: Angular distribution of detected $\Upsilon(1S)$ on-peak

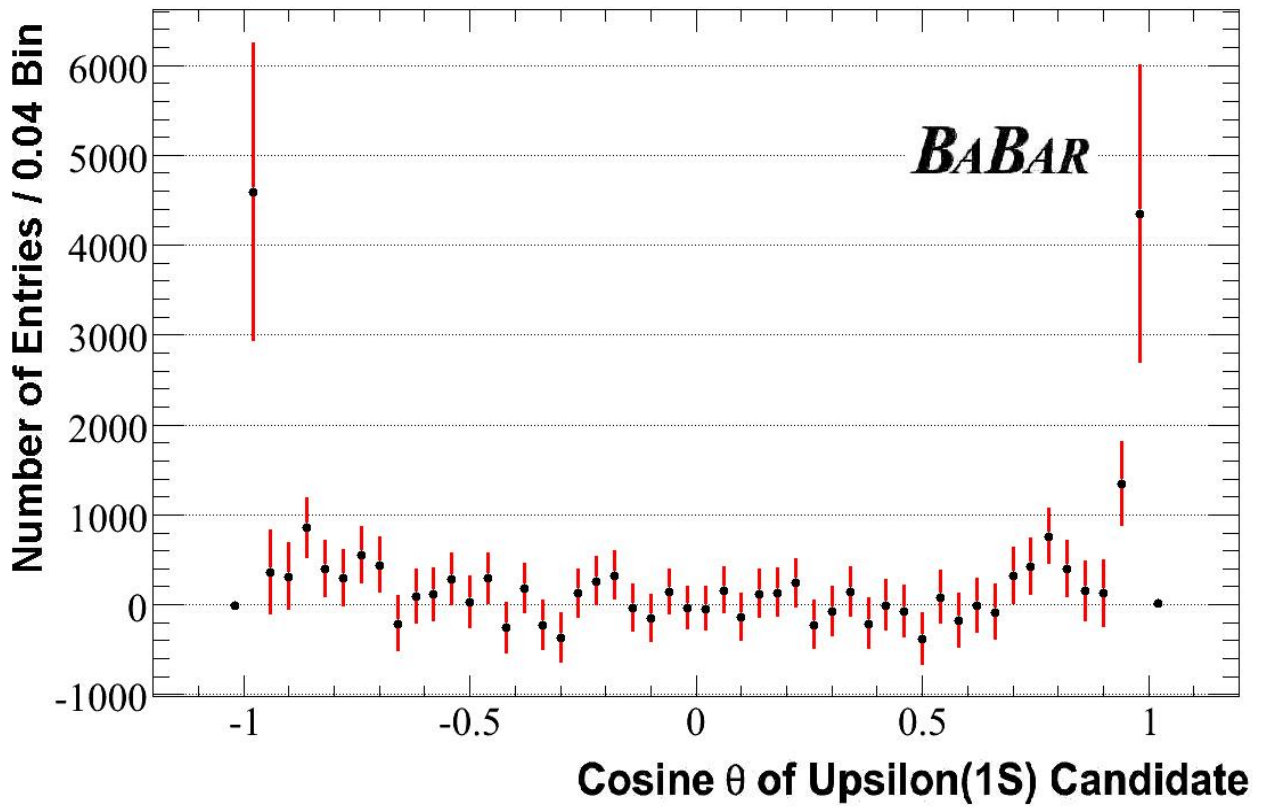


Figure 4.9: Angular distribution of detected $\Upsilon(1S)$ off-peak

$$\sigma_{\gamma_{ISR}\Upsilon(nS)}(s) = \frac{12\pi^2\Gamma_{ee}}{M(nS)s} W(s, 1 - \frac{M^2(nS)}{s}) \quad (4.2)$$

$$x = 1 - \frac{M^2(nS)}{s} \quad (4.3)$$

$$W(s, x) = \Delta\beta x^{\beta-1} - \frac{\beta}{2}(2-x) + \frac{\beta^2}{8} \left\{ (2-x)[3\ln(1-x) - 4\ln x] - 4\frac{\ln(1-x)}{x} - 6 + x \right\} \quad (4.4)$$

$$\Delta = 1 + \frac{\alpha}{\pi} \left(\frac{3}{2}L + \frac{1}{3}\pi^2 - 2 \right) + \left(\frac{\alpha}{\pi} \right)^2 \delta_2 \quad (4.5)$$

$$\delta_2 = \left(\frac{9}{8} - 2\zeta_2 \right) L^2 - \left(\frac{45}{16} - \frac{11}{2}\zeta_2 - 3\zeta_3 \right) L - \frac{6}{5}\zeta_2^2 - \frac{9}{2}\zeta_3 - 6\zeta_2 \ln 2 + \frac{3}{8}\zeta_2 + \frac{57}{12} \quad (4.6)$$

$$\beta = \frac{2\alpha}{\pi} (L - 1) \quad (4.7)$$

$$\zeta_2 = 1.64493407 \quad (4.8)$$

$$\zeta_3 = 1.2020569 \quad (4.9)$$

$$L = 2\ln \frac{\sqrt{s}}{m_e} \quad (4.10)$$

m_e is the mass of an electron. \sqrt{s} is the centre of mass energy. Γ_{ee} is the dielectron width. $M(nS)$ is the mass of an $\Upsilon(nS)$. β in the above equations is not the fraction of the speed of light.

Plugging in the on-peak and off-peak centre of mass energies and the Υ masses gives the cross section for the interactions. Multiplying this by the integrated luminosities and efficiency of each run gives the number of $\Upsilon(1S)$ that we expect to detect. Table 4.2 lists the dielectron widths and ISR cross sections for different Υ . Table 4.3 lists the number of Υ we expect to be produced and the number of $\Upsilon \rightarrow \mu^+\mu^-$ events.

	Dielectron width Γ_{ee} (keV) [3]	On-peak ISR cross section (pb)	Off-peak ISR cross section (pb)
$\Upsilon(1S)$	1.340 ± 0.0018	19.60	20.42
$\Upsilon(2S)$	0.612 ± 0.011	17.11	18.48
$\Upsilon(3S)$	0.272 ± 0.008	28.63	34.54

Table 4.2: Υ dielectron widths and ISR cross sections.

	$\mathcal{B}(\Upsilon \rightarrow \mu^+\mu^-)(\%)$	On-peak ISR Υ	$\Upsilon \rightarrow \mu^+\mu^-$	Off-peak ISR Υ	$\Upsilon \rightarrow \mu^+\mu^-$
$\Upsilon(1S)$	2.48 ± 0.05	8300352	205849	896340	22229
$\Upsilon(2S)$	1.93 ± 0.17	7246524	139858	810872	15650
$\Upsilon(3S)$	2.18 ± 0.21	12124269	264309	1516103	33051

Table 4.3: Number of ISR Υ produced and decayed into muon pairs.

4.6.2 Feed Down Events

In both on-peak and off-peak, there are millions of ISR $\Upsilon(nS)$. The $\Upsilon(2S)$ and $\Upsilon(3S)$ could decay into an $\Upsilon(1S)$. Some of these decays have precisely measured branching fractions. It turns out that the number of $\Upsilon(1S)$ from a cascade of feed down decays is very comparable to the ISR $\Upsilon(1S)$ events. Table 4.4 sums up the known decays from higher mass bottomonium species.

Origin	On-peak feed down $\Upsilon(1S)$	Off-peak feed down $\Upsilon(1S)$
$\Upsilon(2S)$	2303525	257760
$\Upsilon(3S)$	1693811	211806
$\Upsilon(4S)$	75788	0
Total	4073124	469566

Table 4.4: Number of $\Upsilon(1S)$ from known feed down events.

The most significant contribution comes from $\Upsilon(2S)$. Roughly, 30% of $\Upsilon(2S)$ decays into an $\Upsilon(1S)$. The total contributions of feed down events add up to almost one half of ISR $\Upsilon(1S)$. The actual contributions should be bigger because there are branching fractions that have not been measured and there may be processes that we do not know of or understand. The feed down from $\Upsilon(4S)$ in off-peak data is zero because there is no $\Upsilon(4S)$.

The Υ from the cascade of decays have a complicated angular distribution because there are many processes involved. Since there is not yet a Monte Carlo for these events, it is very difficult to model the detection efficiency of these events.

We predict the angular distribution of these to have a preference in the forward and backwards directions but not as sharply peaked. This is because ISR $\Upsilon(2S)$ and $\Upsilon(3S)$ have momentum in the centre of mass frame. Their daughters inherit some of the momentum. Υ also have no preferred decay direction, so the combined effect of these two would make a distribution preferred forward and backwards.

Chapter 5

Results

5.1 Comparison of On-peak and Off-peak Data

Although the energy resolution of the *BABAR* detector was estimated to be 70MeV , the on-peak Gaussian fit at the $\Upsilon(1S)$ region has a width of $(61 \pm 2)\text{MeV}$ and the off-peak has a width of $(48 \pm 5)\text{MeV}$. This may mean that the resolution is different for on-peak and off-peak or there is some process data that we do not know about in the on-peak data set that smeared out the data.

The angular distributions of $\Upsilon(1S)$ in the both on-peak data and off-peak data have very similar shapes and are both peaked in the forwards and backwards direction. This indicates that the on-peak $\Upsilon(1S)$ are mostly created in the same mechanism as off-peak.

The ratio of luminosities between on-peak and off-peak data is $R = 9.7$. Scaling the number of off-peak $\Upsilon(1S)$ by this ratio gives a good estimate of how many $\Upsilon(1S)$ in the on-peak data did not originate from an $\Upsilon(4S)$.

$$N = n\epsilon\mathcal{B} \quad (5.1)$$

$$n = \frac{N}{\epsilon\mathcal{B}} \quad (5.2)$$

$$n' = \frac{N'}{\epsilon\mathcal{B}} \quad (5.3)$$

N is the number of detected $\Upsilon(1S)$ on-peak. n is the number of produced $\Upsilon(1S)$ on-peak. N' is the number of detected $\Upsilon(1S)$ off-peak. n' is the number of produced $\Upsilon(1S)$ off-peak. ϵ is the detection efficiency. \mathcal{B} is the branching fraction of $\Upsilon(1S) \rightarrow \mu^+\mu^-$.

The number of $\Upsilon(1S)$ that originated from a $\Upsilon(4S)$ is therefore

$$\delta = n - n'Rr \quad (5.4)$$

$$\delta = \frac{N - N'Rr}{\epsilon\mathcal{B}} \quad (5.5)$$

r is a correction factor of 0.96, which is equal to the ratio of $\Upsilon(1S)$ ISR cross section on-peak to off-peak. δ corresponds to $1.1 \times 10^7 - 1.0 \times 10^7 \approx 1 \times 10^6$.

To avoid the complications from efficiencies, branching fractions, different resolution widths, and uncertainties, we can simply compare the ratio of detected on-peak events and off peak events. Efficiencies and branching fractions cancel in their ratio $N/(N'Rr)$. This becomes $164400/(9.7 \times 16120 \times 0.96) \approx 1.10$. In other words, just by tuning the centre of mass energy up to the mass of an $\Upsilon(4S)$, we get roughly 10% more $\Upsilon(1S)$ due to $\Upsilon(4S)$ decays.

On-peak and off-peak data both agree that most of the $\Upsilon(1S)$ came from ISR production. The decay $\Upsilon(4S) \rightarrow \Upsilon(1S)$ must happen at some level. This process is small compared to the ISR production of $\Upsilon(1S)$.

5.2 Error Analysis

The three fundamental quantities measured are the total number of $\Upsilon(1S)$, the number of this that originated from an $\Upsilon(4S)$, and how many more $\Upsilon(1S)$ we get if we go from off-peak to on-peak. The uncertainties involved in these calculations are given in Table 5.1.

Parameter	Uncertainty
Ratio of luminosities	1%
$\mathcal{B}(\Upsilon(1S) \rightarrow \mu^+ \mu^-)$	1%
N	2.3%
N'	7.0%
Systematic error between data and Monte Carlo	4%
Detection efficiencies	1.6%
Number of $\Upsilon(4S)$ in on-peak data	1.1%
Systematic error of ratio of ISR luminosities	$\approx 1\%$

Table 5.1: Summary of uncertainties.

Therefore, $n = (1.10 \pm 0.03) \times 10^7$, $\delta = (1.0 \pm 0.9) \times 10^6$, and increasing the centre of mass energy from off-peak to on-peak makes $(10 \pm 8)\%$ more $\Upsilon(1S)$. The uncertainty on δ is huge because $N \approx N' Rr$. Of the 4.65×10^8 $\Upsilon(4S)$, $0.22 \pm 0.18\%$ eventually end up as an $\Upsilon(1S)$. Compared to the branching fraction of $\Upsilon(4S) \rightarrow \Upsilon(1S) + \text{anything} < 0.4\%$ [3], this means that $\Upsilon(4S)$ decayed into $\Upsilon(1S)$ directly most of the time instead of by a cascade of decays.

5.3 Attempt to Measure χ_{bJ} (3P)

$\Upsilon(4S)$ decays into $B\bar{B}$ almost all the time. Approximately 1 million out of the 465 million $\Upsilon(4S)$ did not decay into $B\bar{B}$, which is about 0.2%. Some of these $\Upsilon(4S)$ may have decayed into the theoretical χ_{bJ} (3P). χ_{bJ} in the (3P) orbital has never been directly observed. The mass of χ_{bJ} is theoretically between the mass of a $\Upsilon(3S)$ and a $\Upsilon(4S)$.

	Mass (GeV)	Energy of photon decayed along (MeV)
χ_{b0} (3P)	10.501	79
χ_{b1} (3P)	10.516	64
χ_{b2} (3P)	10.526	54

Table 5.2: χ_{bJ} (3P) masses and energy of the photon that decayed with it.

Daughters in a 2-body decay in the centre of mass frame of the parent have energies

$$E_{daughter1} = \frac{M_{parent}^2 - m_{daughter1}^2 + m_{daughter2}^2}{2M_{parent}m_{daughter1}} \quad (5.6)$$

Therefore, photons decayed with χ_{bJ} (3P) should have energies approximately from 50 to 80MeV in the decay $\Upsilon(4S) \rightarrow \gamma\chi_{bJ}(3P)$. This is difficult to distinguish from the background because there are many background photons that did not originate from the electron, the positron, or their collision. These background photons also have energies in the order of tens of MeV. Theoretically, χ_{bJ} (3P) may also decay radiatively into an $\Upsilon(1S)$. The higher mass difference between χ_{bJ} (3P) and $\Upsilon(1S)$ corresponds to a higher energy photon in the order of 1GeV. Unfortunately, this was also very difficult to distinguish from the background. This is because in the event $e^+e^- \rightarrow \gamma\mu^+\mu^-$, one photon emission events contribute the more than multi-photon events. These one photon events also have photon energies in the order of 1GeV in the χ_{bJ} (3P) rest frame. It is very difficult to resolve background QED photons and χ_{bJ} photons. Besides, the masses of χ_{bJ} (3P) are already very close to each other.

We attempted to measure a χ_{bJ} (3P) by plotting the invariant mass of the two muon plus one photon with energy more than 500MeV. This selection was done to avoid any background photons. If there were χ_{bJ} (3P) in the data, there should be excess events at the theoretical χ_{bJ} (3P) masses.

To do this, the same approach used to plot the angular distributions was used. Figure 5.1 shows plots at the lower region and upper region of the invariant muon pair mass. Then we used the same weighting factors which we used before (53% and 47%) to emulate the signal region. The resulting plot is also given in Figure 5.1. Most of these events are background events. The χ_{bJ} (3P) signal is probably too small and undistinguishable.

5.4 Attempt to Measure $\Upsilon(2S)$ and $\Upsilon(3S)$

We originally proposed to measure $\Upsilon(2S)$ and $\Upsilon(3S)$ too. From the expected events calculation in chapter 4, we can expect that $\Upsilon(2S)$ and $\Upsilon(3S)$ get created in similar amounts by ISR but differ in the feed down contributions. At the $\Upsilon(2S)$ and $\Upsilon(3S)$ regions, there are many more background events compared to the $\Upsilon(1S)$ region. Excess events are more difficult to be seen. Also, the Monte Carlo and data do not agree as well as it did at the $\Upsilon(1S)$ region. The analysis methods used in this study would not work well for a measurement of $\Upsilon(2S)$ and $\Upsilon(3S)$. Figures 5.2 and 5.3 shows how Υ are not distinguishable from the on-peak data. We do not see ‘‘Gaussian bumps’’ at $M_{\Upsilon(2S)}$ or $M_{\Upsilon(3S)}$.

Figure 5.4 is data minus background Monte Carlo on-peak and Figure 5.5 is data minus background Monte Carlo off-peak. In both of these plots, Monte Carlo predicts too few events above the mass region of $\Upsilon(2S)$. These fits were obtained by fitting a Gaussian plus a third order polynomial. It would be difficult to look at the angular distribution of $\Upsilon(2S)$ candidates until we have Monte Carlo that agrees with data better.

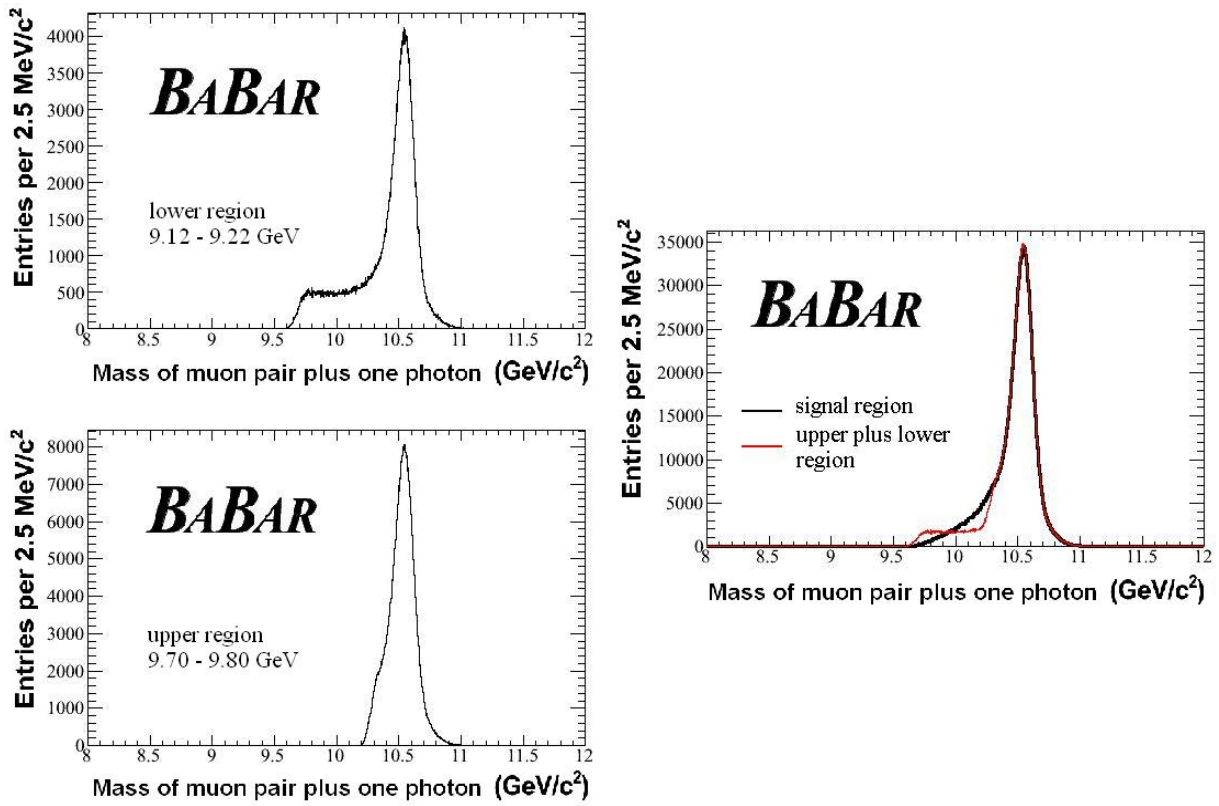


Figure 5.1: Invariant mass of two muons plus one photon greater than 500MeV

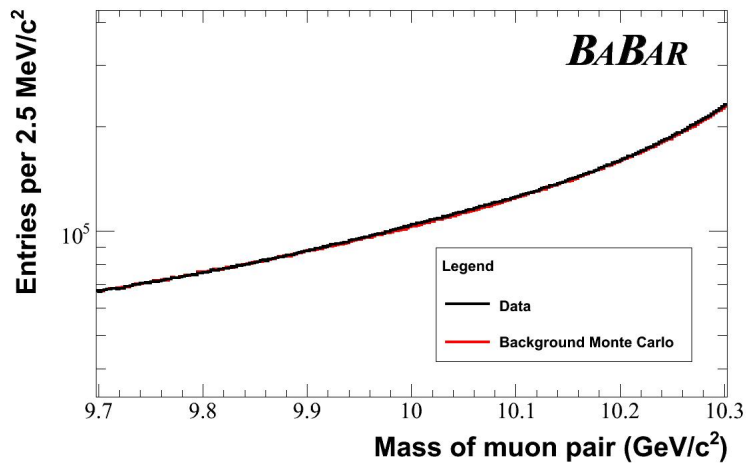
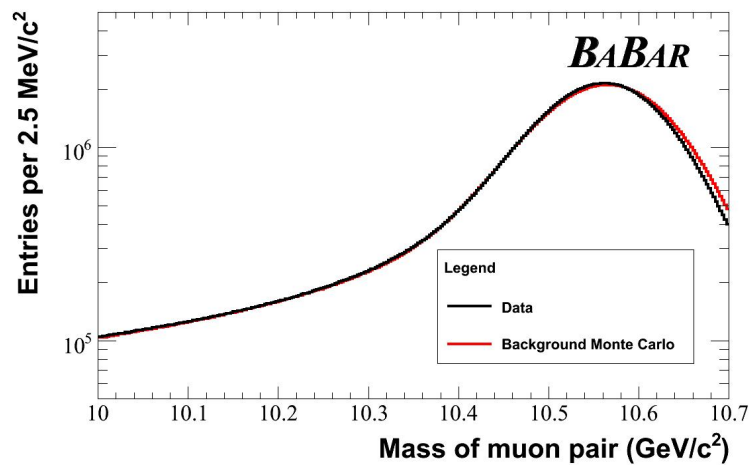
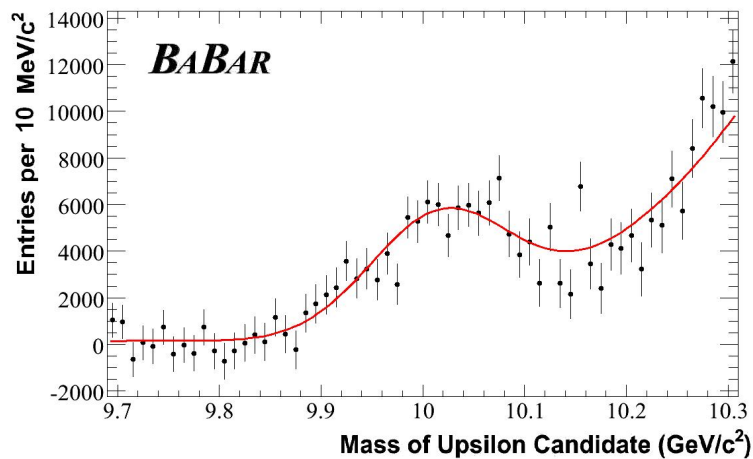


Figure 5.2: On-peak data and background Monte Carlo at $\Upsilon(2S)$ region.

Figure 5.3: On-peak data and background Monte Carlo at $\Upsilon(3S)$ region.Figure 5.4: On-peak data minus background Monte Carlo at $\Upsilon(2S)$ region.

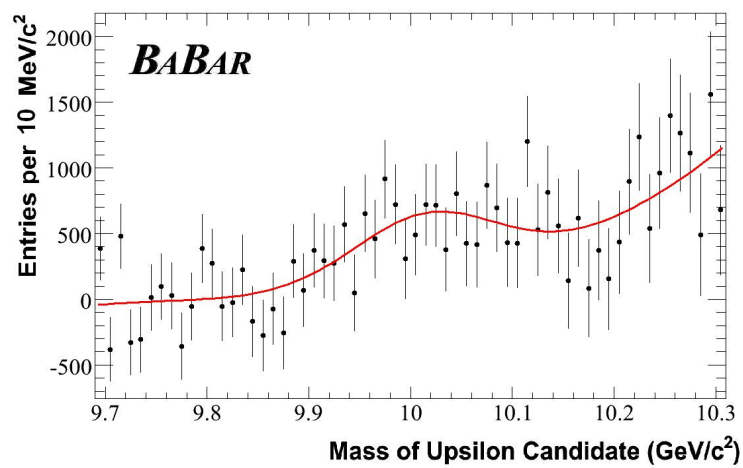


Figure 5.5: Off-peak data minus background Monte Carlo at $\Upsilon(2S)$ region.

Bibliography

- [1] Workbook for BABAR Offline Users.
<http://www.slac.stanford.edu/BFROOT/www/doc/workbook/detector/detector.html>
- [2] Pedlar Todd K. Contribution to the proceedings for "Heavy Quarks and Leptons 2006" (HQL06), 16-20 Oct 2006 Munich, Germany.
- [3] W.-M. Yao et al. (Particle Data Group), J. Phys. G 33, 1 (2006) (URL: <http://pdg.lbl.gov>)
- [4] Griffiths, D. Introduction to elementary particles. New York : J. Wiley and Sons, Inc., 1987.
- [5] *BABAR* Collaboration, B. Aubert et al., Phys. Rev. Lett. 96, 232001 (2006).
- [6] Perkins, Donald H. Introduction to high energy physics. Cambridge ; New York : Cambridge University Press, 2000.
- [7] The *BABAR* Physics Book. <http://www.slac.stanford.edu/pubs/slacreports/slac-r-504.html>
- [8] ROOT: An Object Oriented Data Analysis Framework. <http://root.cern.ch/>
- [9] Patrignani, Claudia. Study of hadronic transitions of $\Upsilon(nS)$ and search for $\Upsilon(nS) \rightarrow \eta \Upsilon(1S)$. *BABAR* Analysis Document # 1784, Version 2. September 25, 2007.
- [10] Benayoun, M. et al. Spectroscopy at B-Factories Using Hard Photon Emission. International Journal of Modern Physics A. arXiv:hep-ph/9910523v1 27 Oct 1999.

Appendix A

Comparison of SP1072 and SP3981

This thesis uses Monte Carlo modenum SP3981 to model $e^+e^- \rightarrow \mu^+\mu^-\gamma$. Both SP1072 and SP3981 model this process. SP3981 is believed to be better at modelling the background muon process, but no one has actually studied their differences. This section compares the two and shows that SP3981 seems better at modelling the actual *BABAR* data.

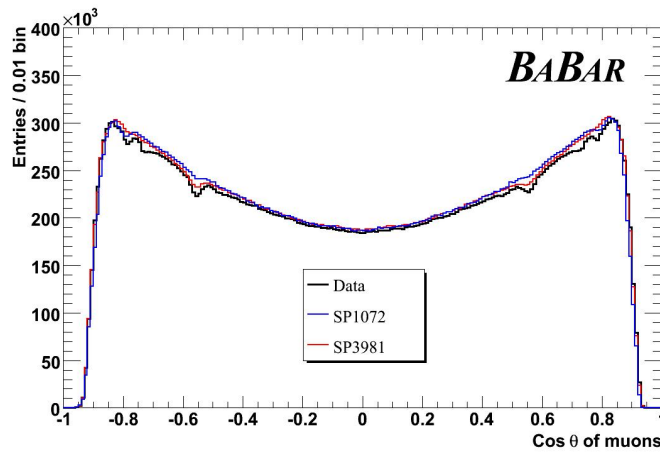


Figure A.1: On-peak comparison of muon angular distribution.

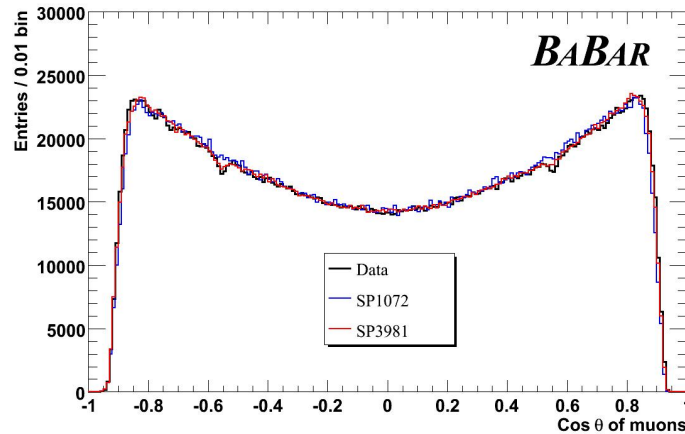


Figure A.2: Off-peak comparison of muon angular distribution.

The muon angular distributions in the Run3 data are compared to SP1072 and Run3 SP3981.

Kolmogorov-Smirnov tests returns a score of 0 between data and SP1072 as well as between data and SP3981. This is possibly due to the small error bars resulting from high statistics. Figure A.1 is on-peak comparison and Figure A.2 is off-peak comparison. Both the Monte Carlo samples have muon angular distributions that are shaped like the data. However, SP3981 appears to resemble data more closely. This is more obvious on-peak than off-peak. SP3981 can also model the detector deficiency more closely at $\cos\theta$ near ± 0.55 . Figure A.3 is a plot of the difference between on-peak data and Monte Carlo samples. Figure A.4 is the corresponding plot for off-peak data. The disagreements appear to be smaller for SP3981.

This is a rather coarse study of the two Monte Carlo modes. More vigorous statistical comparisons can be done to quantify how much better SP3981 is compared to SP1072.

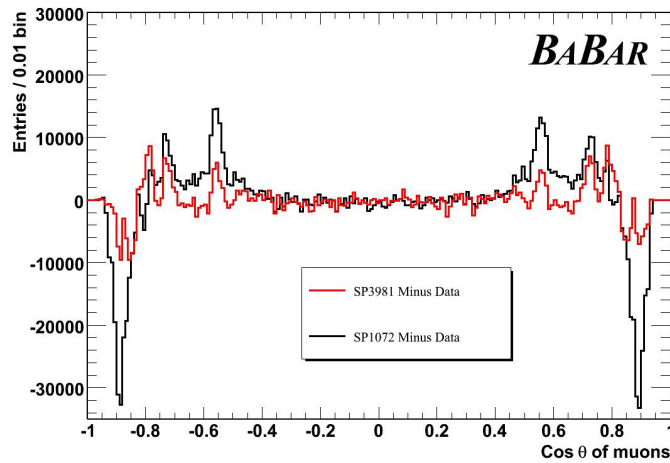


Figure A.3: On-peak differences of muon angular distribution between data and Monte Carlo.

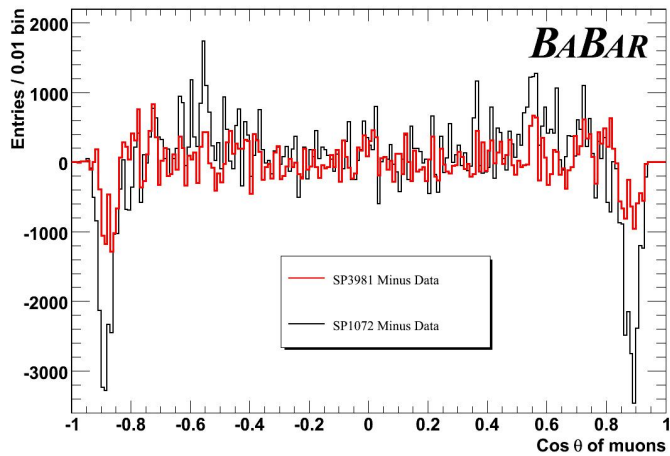


Figure A.4: Off-peak differences of muon angular distribution between data and Monte Carlo.